J. Math. Study
doi: 10.4208/jms.v52n3.19.03

Vol. **52**, No. 3, pp. 258-276
September 2019

Reduced-Order Modelling for the Allen-Cahn Equation Based on Scalar Auxiliary Variable Approaches

Xiaolan Zhou[1], Mejdi Azaiez[1,2] and Chuanju Xu[1,2,*]

[1] *School of Mathematical Sciences and Fujian Provincial Key Laboratory of Mathematical Modeling and High Performance Scientific Computing, Xiamen University, Xiamen 361005, P.R. China.*
[2] *Bordeaux INP, I2M (UMR CNRS 5295), Université de Bordeaux, 33607 Pessac, France.*

Received January 28, 2019; Accepted February 26, 2019

Abstract. In this article, we study the reduced-order modelling for Allen-Cahn equation. First, a collection of phase field data, i.e., an ensemble of snapshots of at some time instances is obtained from numerical simulation using a time-space discretization. The full discretization makes use of a temporal scheme based on the scalar auxiliary variable approach and a spatial spectral Galerkin method. It is shown that the time stepping scheme is unconditionally stable. Then a reduced order method is developed using by proper orthogonal decomposition (POD) and discrete empirical interpolation method (DEIM). It is well-known that the Allen-Cahn equations have a nonlinear stability property, i.e., the free-energy functional decreases with respect to time. Our numerical experiments show that the discretized Allen-Cahn system resulting from the POD-DEIM method inherits this favorable property by using the scalar auxiliary variable approach. A few numerical results are presented to illustrate the performance of the proposed reduced order method. In particular, the numerical results show that the computational efficiency is significantly enhanced as compared to directly solving the full order system.

AMS subject classifications: 76T10, 78M34, 74S25
Key words: Allen-Cahn equation, scalar auxiliary variable, proper orthogonal decomposition, discrete empirical interpolation method.

1 Introduction and motivations

Reduced-Order Model (ROM) applied to numerical design in modern engineering is a tool that is wide-spreading in the scientific community. It is particularly useful in solv-

*Corresponding author. *Email addresses:* xlzhou@stu.xmu.edu.cn (X. Zhou), azaiez@enscbp.fr (M. Azaiez), cjxu@xmu.edu.cn (C. Xu)

ing complex realistic multi-parameters, multi-physics and multi-scale problems, where classical methods such as Finite Difference, Finite Element, and Finite Volume methods would require up to billions of unknowns. On the contrary, ROM is based on a sharp offline/online strategy, which can be realized with a reduced number of unknowns. Such a strategy can be used to handle control, optimization, prediction, and data analysis problems in almost real-time, that is, ultimately, a major goal for industrials. The reduced order modeling offline strategy relies on proper choices for data sampling and construction of the reduced basis, which will be used then in the online phase, where a proper choice of the reduced model describing the dynamic of the system is needed. The key feature of ROM is its capability to drastically reduce the computational cost of numerical simulations, and thus highly speedup computations without compromising too much the physical accuracy of the solution from the engineering point of view. Among the most popular ROM approaches, Proper Orthogonal Decomposition (POD) strategy provides optimal (from the energetic point of view) basis or modes to represent the dynamics from a given database (snapshots) obtained by a full-order system. Onto these reduced basis, a Galerkin projection of the governing equations can be employed to obtain a low-order dynamical system for the basis coefficients. The resulting low-order model is named standard POD-ROM, which thus consists in the projection of high-fidelity (full-order) representations of physical problems onto low-dimensional spaces of solutions, with a dramatically reduced dimension. The main advantage of POD-ROM is that these low-dimensional spaces are capable of capturing the dominant characteristics of the solution, and the computations in the low-dimensional space can be done at a reduced cost. This advantage has led researchers to apply POD to a variety of physical and engineering problems, including the Navier Stokes equations in computational fluid dynamics; See e.g. [2–4] and [8].

We aim in this paper at applying this reduced-order model strategy to solve the Allen-Cahn equation and investigating its efficiency in terms of stability, convergence, and data reduction.

The Allen-Cahn equation was originally introduced to describe the motion of anti-phase boundaries in crystalline solids [1], and has now been used to model many moving interface problems from fluid dynamics to materials science via a phase-field approach. It consists in finding $\phi:\Omega\times(0,T]\to\mathbb{R}$ solution of

$$\begin{cases} \frac{\partial\phi}{\partial t}+\gamma\big(-\Delta\phi+f(\phi)\big)=0, & \forall(\boldsymbol{x},t)\in\Omega\times(0,T], \\ \nabla\phi\cdot\boldsymbol{n}\big|_{\partial\Omega}=0, & \forall t\in(0,T], \\ \phi(t=0)=\phi^0(\boldsymbol{x}), & \forall\boldsymbol{x}\in\Omega. \end{cases} \tag{1.1}$$

In the above, γ is a positive kinetic coefficient, $\Omega\subset\mathbb{R}^d$ is a bounded domain, $\boldsymbol{n}$ is the outward normal, $f(\phi)=F'(\phi)$ with the given function $F(\phi)=\frac{1}{4\varepsilon^2}(\phi^2-1)^2$ being the Ginzburg-

Landau double-well potential. The phase field ϕ is such that

$$\phi = \begin{cases} 1, & \text{phase 1,} \\ -1, & \text{phase 2,} \end{cases}$$

and ε represents the thickness of the smooth transition layer connecting the two phases, which is small compared to the characteristic length of the system scale. The homogeneous Neumann boundary condition implies that no mass loss occurs across the boundary walls.

In the literature, there are only three papers dealing with the reduced order modeling for the Allen-Cahn equation [8, 12, 15]. In the literature, they used convex splitting methods and implicit energy stable methods for time discretization, which require solving nonlinear system or linear system with variable coefficients. While we use scalar auxiliary variable (SAV) scheme [11, 14] to construct full order system, which is unconditionally energy stable and extremely efficient in the sense that only decoupled equations with constant coefficients need to be solved at each time step. And we construct the ROM based on SAV, which inherits all the advantages of SAV.

The small positive parameter ε and the nonlinear term make the Allen-Cahn equation very stiff, and it is computationally expensive to solving the Allen-Cahn equation. To overcome the difficulty and significantly improve the computational efficiency, we develop in this paper a reduced-order modelling for this equation. In our method, the phase field data sampling is first obtained from a numerical method constructed based on the scalar auxiliary variable (SAV) approach for the time discretization and spectral method for the space discretization. The SAV, recently introduced and analyzed by a number of researchers; see, e.g., [14] and the references therein, is an efficient and robust framework to design stable schemes for a large class of gradient flows. The advantage of this approach is that it is not restricted to specific forms of the nonlinear part of the free energy and only requires solving simple decoupled linear equations with constant coefficients. In this work, we apply the SAV approach to construct unconditionally second-order stable scheme for time discretization, and the spectral Galerkin method for space discretization. Once the snapshot sampling is computed from solving the full order system, a set of reduced basis are then obtained by applying POD to the snapshots. In order to reduce the computational complexity in the evaluation of the nonlinear term, we will use the Discrete Empirical Interpolation Method (DEIM) approach [5] to approximate the nonlinear function. Finally, a reduced order system is derived based on the POD basis and DEIM for the nonlinear term. The final reduced order system to be solved has a size much smaller than the full order system.

The rest of the paper is organized as follows. In Section 2, We briefly describe the Proper Orthogonal Decomposition method and Discrete Empirical Interpolation Method. Section 3 is first devoted to present the full discretization method for the Allen-Cahn equation. The SAV-based unconditionally stable scheme for the time discretization and the spectral method for the space discretization are proposed. Then the reduced order

system is derived using POD and DEIM to the snapshot sampling computed from the full order system. In Section 4, several numerical examples are provided to confirm some theoretical results and demonstrate the performance of the proposed algorithm. Finally, some comments and concluding remarks are given in Section 5.

2 Phase-field POD-ROM description

We briefly describe the POD method. For a detailed presentation, the reader is referred to, e.g., [9,13,16].

Let us consider an ensemble of snapshots $\chi=\text{span}\{\phi(\cdot,t_0),\ldots,\phi(\cdot,t_{N_\tau})\}$, which is a collection of phase field data from numerical simulation results of (1.1) at time $t_n=n\Delta t$, $n=0,1,\ldots,N_\tau$ and $\Delta t=T/N_\tau$. In practical applications, these snapshots can be computed with very large time step size Δt, thus the pre-computation cost is very limited. The POD method seeks a low-dimensional basis $\{\psi_1,\ldots,\psi_r\}$ in an Hilbert space $\mathcal{H}$ that optimally approximates the snapshots in the following sense:

$$\min_{\psi_1,\ldots,\psi_r\in\mathcal{H}}\frac{1}{N_\tau+1}\sum_{n=0}^{N_\tau}\left\|\phi(\cdot,t_n)-\sum_{i=1}^{r}(\phi(\cdot,t_n),\psi_i)_{\mathcal{H}}\psi_i\right\|_{\mathcal{H}}^2, \tag{2.1}$$

subject to the condition $\left(\psi_j,\psi_i\right)_{\mathcal{H}}=\delta_{ij}$, $1\le i,j\le r$, where δ_{ij} is the Kronecker delta. To solve the optimization problem (2.1), one can consider the eigenvalue problem:

$$Kz_i=\lambda_i z_i,\quad \text{for } 1,\ldots,r, \tag{2.2}$$

where $K\in\mathbb{R}^{(N_\tau+1)\times(N_\tau+1)}$ is the snapshots correlation matrix with entries:

$$K_{mn}=\frac{1}{N_\tau+1}(\phi(\cdot,t_n),\phi(\cdot,t_m))_{\mathcal{H}},\quad \text{for } m,n=0,\ldots,N_\tau,$$

z_i is the i-th eigenvector, and λ_i is the associated eigenvalue. The eigenvalues are positive and sorted in descending order $\lambda_1\ge\ldots\ge\lambda_r>0$. It can be shown that the solution of (2.1), i.e. the POD basis functions, is given by:

$$\psi_i(\cdot)=\frac{1}{\sqrt{\lambda_i}}\sum_{n=0}^{N_\tau}(z_i)_n\phi(\cdot,t_n),\quad 1\le i\le r, \tag{2.3}$$

where $(z_i)_n$ is the n-th component of the eigenvector z_i. It can also be shown that the following POD error formula holds [9]:

$$\frac{1}{N_\tau+1}\sum_{n=0}^{N_\tau}\left\|\phi(\cdot,t_n)-\sum_{i=1}^{r}(\phi(\cdot,t_n),\psi_i)_{\mathcal{H}}\psi_i\right\|_{\mathcal{H}}^2=\sum_{i=r+1}^{r_K}\lambda_i, \tag{2.4}$$

where r_K is the rank of K.

We consider the following space for the POD setting:

$$X_r = \text{span}\{\psi_1,\ldots,\psi_r\}. \tag{2.5}$$

It is notable that since, as shown in (2.3), the POD basis functions are linear combinations of the snapshots, the POD basis functions satisfy the boundary conditions in (1.1).

The Galerkin projection-based POD-ROM makes use of both Galerkin truncation and Galerkin projection. The former yields an approximation of the phase field by a linear combination of the truncated POD basis:

$$\phi(\boldsymbol{x},t) \approx \phi_r(\boldsymbol{x},t) = \sum_{i=1}^{r} a_i(t)\psi_i(\boldsymbol{x}), \tag{2.6}$$

where $\{a_i(t)\}_{i=1}^r$ are the sought time-varying coefficients representing the POD-Galerkin trajectories. Note that $r \ll \mathcal{N}$, where $\mathcal{N}$ denotes the number of degrees of freedom in a full order simulation. Replacing the phase field function ϕ with ϕ_r in the equation (1.1), using the Galerkin method, and projecting the resulted equations onto the space X_r, one obtains the standard POD-ROM for the Allen-Cahn equation:

Find $\phi_r \in X_r$ such that

$$(\partial_t \phi_r,\psi) + \gamma((\nabla\phi_r,\nabla\psi) + (f(\phi_r),\psi)) = 0 \quad \forall \psi \in X_r, \tag{2.7}$$

and $\phi_r(\cdot,0) = \phi_r^0$ which is the projection of ϕ^0 into X_r.

2.1 A problem with complexity of the POD-Galerkin approach

This subsection illustrates the computational inefficiency that may occur in solving the reduced order system (2.7) from the standard POD-Galerkin approach. We denote $\boldsymbol{a}(t) = [a_1(t),\ldots,a_r(t)]^T$ is the coefficient vector of the reduced solution. The coefficient vectors of the reduced basis function expanded by basis functions of X_N defined in (3.10) are collected in the columns of the matrix $\boldsymbol{\Psi}_r = [\Psi_{\cdot,1},\ldots,\Psi_{\cdot,r}] \in \mathbb{R}^{\mathcal{N}\times r}$, i.e.,

$$\psi_k(x,y) = \sum_{i,j=0}^{N} \psi_k(\xi_i,\xi_j) h_i(x) h_j(y),$$

and $\Psi_{\cdot,k}$, $k=1,\ldots,r$ are vectors of length $\mathcal{N} := (N+1)^2$ formed by the $\psi_k(\xi_i,\xi_j)$. Equation (2.7) in vector version conclude the following nonlinear term:

$$\underbrace{\boldsymbol{\Psi}_r^T \boldsymbol{W}}_{r\times\mathcal{N}} \underbrace{\boldsymbol{f}(\boldsymbol{\Psi}_r \boldsymbol{a}(t))}_{\mathcal{N}\times 1}, \tag{2.8}$$

where weighted matrix $\boldsymbol{W} \in \mathbb{R}^{\mathcal{N}\times\mathcal{N}}$ is a symmetric, positive-definite matrix. This nonlinear term has a computational complexity that depends on $\mathcal{N}$, where $\mathcal{N}$ is the dimension

of the original full-order system (2.1). It requires the order of $2r\mathcal{N}$ flops for matrix-vector multiplications, and a full evaluation of the nonlinear function $\boldsymbol{f}$ at the $\mathcal{N}$-dimensional vector $\boldsymbol{\Psi}_r\boldsymbol{a}(t)$. In particular, supposing that the complexity for evaluating the nonlinear function $\boldsymbol{f}$ with q components is $O(c(q))$, where c is some function of q, then the complexity for computing (2.8) is roughly $O(c(\mathcal{N})+4r\mathcal{N})$. Here, the $4r\mathcal{N}$ flops are a result of the two matrix-vector products required to form the argument of f and then to form the projection. That means that the reduced-order model is not independent of the full dimension $\mathcal{N}$. As a result, solving this reduced-order model might still be computationally expensive (probably as expensive as solving the original system).

2.2 Discrete Empirical Interpolation Method (DEIM) for nonlinear terms

In order to reduce the computational complexity of POD-ROM for time dependent and/or parameterized nonlinear partial differential equations, a discrete empirical interpolation method (DEIM) was proposed in Chaturantabut and Sorensen [5]. The main idea of DEIM is to provide an approximation to the nonlinear terms of ODE systems in a form that enables precomputation of certain matrices so that the computational cost of evaluating the nonlinear terms is greatly decreased and becomes independent of the original dimension $\mathcal{N}$. This approximation is realized by computing the basis using a POD approach combined with a greedy algorithm.

To apply this idea, we approximate the nonlinear function $\boldsymbol{f}\big(\boldsymbol{\Psi}_r\boldsymbol{a}(t)\big)$ by projecting it into the subspace spanned by a basis $\{\boldsymbol{u}_1,...,\boldsymbol{u}_p\}\subset\mathbb{R}^{\mathcal{N}}$ of dimension $p\ll\mathcal{N}$ so that the approximation takes the form

$$\boldsymbol{f}\big(\boldsymbol{\Psi}_r\boldsymbol{a}(t)\big)\approx\boldsymbol{U}\boldsymbol{f}_{\boldsymbol{p}}(t), \tag{2.9}$$

where $\boldsymbol{U}=[\boldsymbol{u}_1,...,\boldsymbol{u}_p]\in\mathbb{R}^{\mathcal{N}\times p}$ and $\boldsymbol{f}_{\boldsymbol{p}}(t)$ is the corresponding coefficient vector, which can be regarded as an approximation to the nonlinear term $\boldsymbol{f}\big(\boldsymbol{\Psi}_r\boldsymbol{a}(t)\big)$. To determine $\boldsymbol{f}_{\boldsymbol{p}}(t)$, we select p distinguished rows from $\boldsymbol{f}\big(\boldsymbol{\Psi}_r\boldsymbol{a}(t)\big)$. To this end, we construct the matrix

$$\boldsymbol{P}=[\boldsymbol{e}_{i_1},...,\boldsymbol{e}_{i_p}]\in\mathbb{R}^{\mathcal{N}\times p}, \tag{2.10}$$

where $\boldsymbol{e}_i=[0,...,0,1,0,...,0]^T\in\mathbb{R}^{\mathcal{N}}$ is the i-th column of the identity matrix $\boldsymbol{I}_{\mathcal{N}}\in\mathbb{R}^{\mathcal{N}\times\mathcal{N}}$ for $i=i_1,...,i_p$. Then we solve $\boldsymbol{f}_{\boldsymbol{p}}(t)$ from the following equation

$$(\boldsymbol{P}^T\boldsymbol{U})\boldsymbol{f}_{\boldsymbol{p}}(t)=\boldsymbol{P}^T\boldsymbol{f}\big(\boldsymbol{\Psi}_r\boldsymbol{a}(t)\big). \tag{2.11}$$

This gives

$$\boldsymbol{f}_{\boldsymbol{p}}(t)=(\boldsymbol{P}^T\boldsymbol{U})^{-1}\boldsymbol{P}^T\boldsymbol{f}\big(\boldsymbol{\Psi}_r\boldsymbol{a}(t)\big). \tag{2.12}$$

Notice that for the nonlinear term in the Allen-Cahn equation, the matrix $\boldsymbol{P}^T$ can be moved inside the function, thus we obtain

$$\begin{aligned}\boldsymbol{f}_{\boldsymbol{p}}(t)\approx\boldsymbol{U}\boldsymbol{f}_{\boldsymbol{p}}(t)&=\boldsymbol{U}(\boldsymbol{P}^T\boldsymbol{U})^{-1}\boldsymbol{P}^T\boldsymbol{f}\big(\boldsymbol{\Psi}_r\boldsymbol{a}(t)\big)\\&=\boldsymbol{Q}\boldsymbol{f}\big(\boldsymbol{P}^T\boldsymbol{\Psi}_r\boldsymbol{a}(t)\big),\end{aligned} \tag{2.13}$$

where we define $\boldsymbol{Q}:=\boldsymbol{U}(\boldsymbol{P}^T\boldsymbol{U})^{-1}$. To summarize, to obtain an approximation to $\boldsymbol{f_p}(t)$, we must construct

- the projection basis $\{\boldsymbol{u}_1,...,\boldsymbol{u}_p\}$;
- the interpolation indices $\{i_1,...,i_p\}$ used in (2.10).

The DEIM algorithm generates the basis using the POD approach. Here the previously introduced POD approach is applied to the snapshots of the nonlinearity $\boldsymbol{f}\big(\boldsymbol{\Psi}_r\boldsymbol{a}(t)\big)$ to compute $\boldsymbol{U}$. The selection for the interpolation points in the algorithms is based on a greedy algorithm. The idea is to successively select spatial points to limit the growth of an error bound. The indices are constructed inductively from the input data as follows. For more details we refer the reader to [5].

Algorithm 2.1. DEIM (POD-greedy algorithm)

Reuire: Snapshots $\boldsymbol{F}=[\boldsymbol{f}(\phi(t_1)),\cdots,\boldsymbol{f}(\phi(t_{N_\tau}))]\in\mathbb{R}^{\mathcal{N}\times N_\tau}$ and rank p;

1: Compute POD basis $[\boldsymbol{u}_1,\cdots,\boldsymbol{u}_p]\in\mathbb{R}^{\mathcal{N}\times p}$ for $\boldsymbol{F}$;

2: $i_1\leftarrow \text{argmax}_{j=1,\cdots,\mathcal{N}}|(\boldsymbol{u}_1)_j|$;

3: $\boldsymbol{U}=[\boldsymbol{u}_1]$, $\boldsymbol{P}=[\boldsymbol{e}_{i_1}]$, ;

4: **for** $k=2$ to p **do**;

5: $\quad\boldsymbol{u}\leftarrow\boldsymbol{u}_k$;

6: $\quad$solve $(\boldsymbol{P}^T\boldsymbol{U})\boldsymbol{f_p}=\boldsymbol{u}$ for $\boldsymbol{f_p}$;

7: $\quad\boldsymbol{r}=\boldsymbol{u}-\boldsymbol{U}\boldsymbol{f_p}$;

8: $\quad i_k\leftarrow\text{argmax}_{j=1,\cdots,\mathcal{N}}|(\boldsymbol{r})_j|$;

9: $\quad\boldsymbol{U}\leftarrow[\boldsymbol{U},\boldsymbol{u}]$, $\boldsymbol{P}\leftarrow[\boldsymbol{P},\boldsymbol{e}_{i_k}]$;

10: **end for**;

11: **return** $\boldsymbol{U}$ and $(i_1,\ldots,i_p)$.

3 Numerical methods

In this section, we propose a brief description of the spatial and temporal approximation methods. These schemes will be used to solve the full problem and produce the snapshots but also the reduced model one.

3.1 Some notations for the spatial discretization

Let $\Sigma=\{(\xi_i,\rho_i);0\le i\le N\}$ denote the sets of Gauss-Lobatto-Legendre quadrature nodes and weights associated to polynomials of degree N (see, [7, 10]). These quantities

are such that on $\Lambda:=]-1,+1[$

$$\forall\phi\in\mathbb{P}_{2N-1}(\Lambda),\qquad \int_{-1}^{+1}\phi(\xi)d\xi=\sum_{j=0}^{N}\phi(\xi_j)\rho_j, \tag{3.1}$$

where $\mathbb{P}_N(\Lambda)$ denotes the space of polynomials of degree $\leq N$. We recall that the nodes $\xi_i(0\leq i\leq N)$ are solution to $(1-x^2)L_N'(x)=0$, where L_N denotes the Legendre polynomial of degree N.

The canonical polynomial interpolation basis $h_i(x)\in\mathbb{P}_N(\Lambda)$ built on Σ is given by the relationships:

$$h_i(x)=-\frac{1}{N(N+1)}\frac{1}{L_N(\xi_i)}\frac{(1-x^2)L_N'(x)}{(x-\xi_i)},\qquad -1\leq x\leq+1,\quad 0\leq i\leq N, \tag{3.2}$$

with the elementary cardinality property

$$h_i(\xi_j)=\delta_{ij},\qquad 0\leq i,j\leq N. \tag{3.3}$$

In the sequel the phase field ϕ in domain $\Omega=\Lambda^2$ will be approximated in space variable by suitable polynomial functions ϕ_N as follows

$$\phi_N(\boldsymbol{x},t)=\sum_{i=0}^{N}\sum_{j=0}^{N}\phi_{i,j}(t)h_i(x)h_j(y). \tag{3.4}$$

The L^2-inner products involved in the calculation will be evaluated using Gauss-Lobatto-Legendre quadrature, which reads: for all continuous functions φ and ψ in $\bar{\Omega}$,

$$(\varphi,\psi)\approx(\varphi,\psi)_N:=\sum_{i=0}^{N}\sum_{j=0}^{N}\varphi(\xi_i)\psi(\xi_j)\rho_i\rho_j. \tag{3.5}$$

3.2 Scalar auxiliary variable (SAV) approach for Allen-Cahn equation

SAV approach was introduced in [14] to solve gradient flows. The main purpose of this section is to construct efficient unconditionally stable scheme based on this approach for (1.1).

Throughout the paper, we assume that the energy part $\int_\Omega F(\phi)\mathrm{d}\boldsymbol{x}$ is bounded from below, that is, there exists a constant C_0 such that $\int_\Omega F(\phi)\mathrm{d}\boldsymbol{x}+C_0>0$. We first introduce a *scalar* auxiliary variable

$$s(t):=\sqrt{\int_\Omega F(\phi)\,\mathrm{d}\boldsymbol{x}+C_0}.$$

Then, we rewrite the phase–field equation (1.1) under an equivalent form as follows: find $\phi:\Omega\times(0,T]\to\mathbb{R}$ and $s:(0,T]\to\mathbb{R}$, such that

$$\begin{cases} \frac{\partial\phi}{\partial t}=-\gamma\mu, \qquad \nabla\phi\cdot\boldsymbol{n}\big|_{\partial\Omega}=0, \\ \mu=-\Delta\phi+\dfrac{s(t)}{\sqrt{\int_\Omega F(\phi)d\boldsymbol{x}+C_0}}f(\phi), \\ \dfrac{\mathrm{d}s(t)}{\mathrm{d}t}=\dfrac{1}{2\sqrt{\int_\Omega F(\phi)d\boldsymbol{x}+C_0}}\displaystyle\int_\Omega f(\phi)\frac{\partial\phi}{\partial t}d\boldsymbol{x}. \end{cases} \tag{3.6}$$

Taking the inner product of the first two equations with μ, $\frac{\partial\phi}{\partial t}$ respectively, and multiplying the third equation with $2s$, then adding them together, we obtain the energy dissipation law for (3.6):

$$\frac{d}{dt}\left(s(t)^2+\frac{1}{2}\|\nabla\phi\|_0^2\right)=-\gamma\int_\Omega\|\mu\|_0^2d\boldsymbol{x}. \tag{3.7}$$

The energy law (3.7) means that the SAV approach (3.6) makes the modified energy

$$H(\phi)=s^2+\frac{1}{2}\|\nabla\phi\|_0^2$$

decays in time.

3.3 Full discretization: full order system

Now we construct the full discretization problem, also termed as full order system (FOS) hereafter, for the Allen-Cahn equation. First, for the temporal discretization, we use the second-order backward difference scheme (BDF2) to the system (3.6).

Let $s^0=\sqrt{\int_\Omega F(\phi^0)d\boldsymbol{x}+C_0}$. Given initial conditions $\phi^0=\phi_0$, find ϕ^{n+1} and $s^{n+1}\in\mathbb{R}$, $n=1,2,\ldots$, such that

$$\begin{cases} \frac{3\phi^{n+1}-4\phi^n+\phi^{n-1}}{2\Delta t}=-\gamma\mu^{n+1}, \\ \mu^{n+1}=-\Delta\phi^{n+1}+\dfrac{s^{n+1}}{\sqrt{\bar{\mathcal{F}}^{n+1}}}f(\bar{\phi}^{n+1}), \\ \dfrac{3s^{n+1}-4s^n+s^{n-1}}{2\Delta t}=\dfrac{1}{2\sqrt{\bar{\mathcal{F}}^{n+1}}}\displaystyle\int_\Omega f(\bar{\phi}^{n+1})\frac{3\phi^{n+1}-4\phi^n+\phi^{n-1}}{2\Delta t}d\boldsymbol{x}, \end{cases} \tag{3.8}$$

where $\bar{\mathcal{F}}^{n+1}=\int_\Omega F(\bar{\phi}^{n+1})d\boldsymbol{x}+C_0$, $\bar{\phi}^{n+1}$ can be any explicit approximation of $\phi(t^{n+1})$ with an error of $\mathcal{O}(\Delta t^2)$. For instance, we may choose the following extrapolation:

$$\bar{\phi}^{n+1}=2\phi^n-\phi^{n-1}.$$

In [11] it has been proved that the scheme (3.8) is second-order accurate, unconditionally stable in the sense that

$$\frac{1}{\Delta t}\Big(\tilde{H}[(\phi^{n+1},s^{n+1}),(\phi^n,s^n)]-\tilde{H}[(\phi^n,s^n),(\phi^{n-1},s^{n-1})]\Big)\leq-\gamma\|\mu^{n+1}\|_0^2, \tag{3.9}$$

where $\tilde{H}$ is the modified energy, defined by:

$$\begin{aligned}&\tilde{H}[(\phi^{n+1},s^{n+1}),(\phi^n,s^n)]\\ :=&\frac{1}{4}\Big(\|\nabla\phi^{n+1}\|_0^2+\|2\nabla\phi^{n+1}-\nabla\phi^n\|^2\Big)+\frac{1}{2}\Big((s^{n+1})^2+(2s^{n+1}-s^n)^2\Big).\end{aligned}$$

The spatial discretization to the semi-discrete problem (3.8) makes use of a spectral-Galerkin method. Let

$$X_N:=\text{span}\Big\{h_i(x)h_j(y);\quad i,j=0,\ldots,N\Big\}. \tag{3.10}$$

I_N is the interpolation operator based on the Legendre Gauss-Lobatto points $\{\xi_i;0\leq i\leq N\}$. Given initial conditions

$$\phi_N^0=I_N\phi_0,\qquad s_N^0:=\sqrt{\int_\Omega F(\phi_N^0)d\boldsymbol{x}+C_0}.$$

Then the spatial discretization consists in seeking the numerical solution ϕ_N^{n+1} in the polynomial space X_N and $s_N^{n+1}\in\mathbb{R},n=0,1,\ldots$, such that, for $\forall\psi\in X_N$,

$$\begin{cases}\Big(\frac{3\phi_N^{n+1}-4\phi_N^n+\phi_N^{n-1}}{2\Delta t},\,\psi\Big)_N=-\gamma\big(\mu^{n+1},\,\psi\big)_N,\\ \big(\mu^{n+1},\,\psi\big)_N=\big(\nabla\phi_N^{n+1},\,\nabla\psi\big)_N+\dfrac{s_N^{n+1}}{\sqrt{\bar{\mathcal{F}}_N^{n+1}}}\big(f(\bar{\phi}_N^{n+1}),\,\psi\big)_N,\\ \dfrac{3s_N^{n+1}-4s_N^n+s_N^{n-1}}{2\Delta t}=\dfrac{1}{2\sqrt{\bar{\mathcal{F}}_N^{n+1}}}\Big(f(\bar{\phi}_N^{n+1}),\,\dfrac{3\phi_N^{n+1}-4\phi_N^n+\phi_N^{n-1}}{2\Delta t}\Big)_N,\end{cases} \tag{3.11}$$

where

$$\bar{\mathcal{F}}_N^{n+1}=\int_\Omega F(\bar{\phi}_N^{n+1})d\boldsymbol{x}+C_0.$$

This full order system can be efficiently solved by the following algorithm; see [14] for more details.

Algorithm 3.1. Implementation of FOS

Require: Given the initial condition ϕ_N^0 and s_N^0. First use a first order method to compute ϕ_N^1 and s_N^1. Then for $n=1,2,\ldots$, we do the following:

1: Set $\bar{\phi}_N^{n+1}=2\phi_N^n-\phi_N^{n-1}$, $\bar{\mathcal{F}}_N^{n+1}=\int_\Omega F(\bar{\phi}_N^{n+1})d\boldsymbol{x}+C_0$, $g^n=\dfrac{4\phi_N^n-\phi_N^{n-1}}{2\gamma\Delta t}-\alpha_1 f(\bar{\phi}_N^{n+1})$, where $\alpha_1=\frac{4s_N^n-s_N^{n-1}}{3\sqrt{\bar{\mathcal{F}}_N^{n+1}}}-\frac{\alpha_0}{2\bar{\mathcal{F}}_N^{n+1}}$, $\alpha_0=\big(f(\bar{\phi}_N^{n+1}),4\phi_N^n-\phi_N^{n-1}\big)_N/3$.

2: Solve: Find $u_N^{n+1}\in X_N$ such that, for $\forall\psi_N\in X_N$,

$$\frac{3}{2\gamma\Delta t}\big(u_N^{n+1},\psi_N\big)_N+\big(\nabla u_N^{n+1},\nabla\psi_N\big)_N=\big(f(\bar{\phi}_N^{n+1}),\psi_N\big)_N.$$

3: Solve: Find $w_N^{n+1}\in X_N$ such that, for $\forall\psi_N\in X_N$,

$$\frac{3}{2\gamma\Delta t}\big(w_N^{n+1},\psi_N\big)_N+\big(\nabla w_N^{n+1},\nabla\psi_N\big)_N=\frac{1}{2\gamma\Delta t}\big(4\phi_N^n-\phi_N^{n-1},\psi_N\big)_N-\alpha_1\big(f(\bar{\phi}_N^{n+1}),\psi_N\big)_N.$$

4: Compute $\phi_N^{n+1}=w_N^{n+1}-\alpha_4 u_N^{n+1}$, $s_N^{n+1}=\dfrac{4s_N^n-s_N^{n-1}}{3}+\dfrac{\big(f(\bar{\phi}_N^{n+1}),\phi_N^{n+1}\big)_N-\alpha_0}{2\sqrt{\bar{\mathcal{F}}_N^{n+1}}}$, where $\alpha_4=\alpha_3/(2\bar{\mathcal{F}}_N^{n+1}+\alpha_2)$, $\alpha_3=\big(f(\bar{\phi}_N^{n+1}),w_N^{n+1}\big)_N$, $\alpha_2=\big(f(\bar{\phi}_N^{n+1}),u_N^{n+1}\big)_N$.

Note that in step 2 & step 3 in the above algorithm, only a linear constant coefficient Poisson equation needs to be solved.

3.4 Reduced-order system

We describe below the construction of the reduced order system through the POD-Galerkin method for the full discrete problem (3.11) and DEIM approach for treating the nonlinear term.

Let us consider an ensemble of snapshots $\chi=\left\{\phi_N^0,\ldots,\phi_N^{N_\tau}\right\}$, which is a collection of phase field data from the numerical solution of (3.11) at time $t_n=n\Delta t$, $n=0,1,\ldots,N_\tau$, $\Delta t=T/N_\tau$. As it is already emphasized in Section 2, these snapshots can be computed with a large time-step size Δt (so with limited pre-computation cost). We use this snapshot set χ to construct the POD basis $\{\psi_1,\ldots,\psi_r\}$, $r\ll\mathcal{N}$, described in Section 2, which is a set of L^2-orthogonal basis functions, such that $(\psi_i,\psi_j)_N=\delta_{ij}$. We also need to precompute the matrix $\boldsymbol{G}$, defined as

$$\boldsymbol{G}=(g_{ij})\in\mathbb{R}^{r\times r},\ \text{with}\ g_{ij}:=(\nabla\psi_i,\nabla\psi_j)_N. \tag{3.12}$$

The reduced-order system is obtained by the following spectral Galerkin method using the approximation space spanned by the POD basis. That is, we seek to project the

solution of the original system onto the space X_r:= span$\{\psi_1,\ldots,\psi_r\}$, so that the projected solution $\phi_r^{n+1}\in X_r$ and $s_r^{n+1}\in\mathbb{R}, n=1,2,\ldots$, satisfy, for $\forall\psi\in X_r$,

$$\begin{cases} \left(\frac{3\phi_r^{n+1}-4\phi_r^n+\phi_r^{n-1}}{2\Delta t},\,\psi\right)_N=-\gamma\left(\mu^{n+1},\,\psi\right)_N, \\ \left(\mu^{n+1},\,\psi\right)_N=\left(\nabla\phi_r^{n+1},\,\nabla\psi\right)_N+\frac{s_r^{n+1}}{\sqrt{\bar{\mathcal{F}}_N^{n+1}}}\left(f(\bar{\phi}_r^{n+1}),\,\psi\right)_N, \\ \frac{3s_r^{n+1}-4s_r^n+s_r^{n-1}}{2\Delta t}=\frac{1}{2\sqrt{\bar{\mathcal{F}}_r^{n+1}}}\left(f(\bar{\phi}_r^{n+1}),\,\frac{3\phi_r^{n+1}-4\phi_r^n+\phi_r^{n-1}}{2\Delta t}\right)_N, \end{cases} \tag{3.13}$$

where $\bar{\mathcal{F}}_r^{n+1}=\int_\Omega F(\bar{\phi}_r^{n+1})d\boldsymbol{x}+C_0$.

The solutions to FOS and ROM are related through the relationship:

$$\boldsymbol{\phi}_N^n\approx\boldsymbol{\phi}_r^n=\boldsymbol{\Psi}_r\boldsymbol{a}^n, \tag{3.14}$$

where $\boldsymbol{\phi}_N^n$ and $\boldsymbol{\phi}_r^n$ are the coefficients vectors of $\phi_N^n(\boldsymbol{x})$ and $\phi_r^n(\boldsymbol{x})$ expanded by the basis functions of X_N, respectively, $\boldsymbol{a}^n$ is the coefficients vector of $\phi_r^n(\boldsymbol{x})$ expanded by the basis functions of X_r. Matrix $\boldsymbol{\Psi}_r$ is defined in Subsection 2.1. It is seen that the columns of $\boldsymbol{\Psi}_r$ are the coefficient vectors of the reduced basis functions expanded by the basis functions of X_N.

Substituting (3.12) and (3.14) into the system (3.13), we obtain, for the unknown coefficient vectors, the reduced-order system: find $\boldsymbol{a}^{n+1}\in\mathbb{R}^r$ and $s_r^{n+1}\in\mathbb{R}, n=1,2,\ldots$, such that,

$$\begin{cases} \frac{3\boldsymbol{a}^{n+1}-4\boldsymbol{a}^n+\boldsymbol{a}^{n-1}}{2\Delta t}=\boldsymbol{G}\boldsymbol{a}^{n+1}+\frac{s_r^{n+1}}{\sqrt{\bar{\mathcal{F}}_r^{n+1}}}\boldsymbol{\Psi}_r^T\boldsymbol{W}\boldsymbol{f}(\boldsymbol{\Psi}_r\bar{\boldsymbol{a}}^{n+1}), \\ 3s_r^{n+1}-4s_r^n+s_r^{n-1}=\frac{1}{2\sqrt{\bar{\mathcal{F}}_r^{n+1}}}\left(\boldsymbol{\Psi}_r^T\boldsymbol{W}\boldsymbol{f}(\boldsymbol{\Psi}_r\bar{\boldsymbol{a}}^{n+1}),\,3\boldsymbol{a}^{n+1}-4\boldsymbol{a}^n+\boldsymbol{a}^{n-1}\right). \end{cases} \tag{3.15}$$

The difficulty here is that the computation of the non-linear term $\boldsymbol{\Psi}_r^T\boldsymbol{W}\boldsymbol{f}(\boldsymbol{\Psi}_r\bar{\boldsymbol{a}}^{n+1})$ depends on the original dimension. Approaching this term by using the DEIM algorithm described in Subsection 2.2, we obtain the final reduced-order problem:

$$\begin{cases} \frac{3\boldsymbol{a}^{n+1}-4\boldsymbol{a}^n+\boldsymbol{a}^{n-1}}{2\Delta t}=\boldsymbol{G}\boldsymbol{a}^{n+1}+\frac{s_r^{n+1}}{\sqrt{\bar{\mathcal{F}}_r^{n+1}}}\boldsymbol{H}\boldsymbol{f}(\boldsymbol{P}^T\boldsymbol{\Psi}_r\bar{\boldsymbol{a}}^{n+1}) \\ 3s_r^{n+1}-4s_r^n+s_r^{n-1}=\frac{1}{2\sqrt{\bar{\mathcal{F}}_r^{n+1}}}\left(\boldsymbol{H}\boldsymbol{f}(\boldsymbol{P}^T\boldsymbol{\Psi}_r\bar{\boldsymbol{a}}^{n+1}),\,3\boldsymbol{a}^{n+1}-4\boldsymbol{a}^n+\boldsymbol{a}^{n-1}\right), \end{cases} \tag{3.16}$$

where $\boldsymbol{H}:=\boldsymbol{\Psi}_r^T\boldsymbol{W}\boldsymbol{Q}\in\mathbb{R}^{r\times p}$ is pre-computed, $\bar{\boldsymbol{a}}^{n+1}:=2\boldsymbol{a}^n-\boldsymbol{a}^{n-1}$, $\bar{\mathcal{F}}_r^{n+1}:=\int_\Omega F(\Psi_r\bar{\boldsymbol{a}}^{n+1})d\boldsymbol{x}+C_0$. Notice that the inter products in the right hand side of (3.16) can be evaluated through the relationship:

$$\left(\boldsymbol{H}\boldsymbol{f}(\boldsymbol{P}^T\boldsymbol{\Psi}_r\bar{\boldsymbol{a}}^{n+1}),\,\boldsymbol{a}^n\right)_{\mathbb{R}^r}=\left(\boldsymbol{W}\boldsymbol{Q}\boldsymbol{f}(\boldsymbol{P}^T\boldsymbol{\Psi}_r\bar{\boldsymbol{a}}^{n+1}),\boldsymbol{\Psi}_r\boldsymbol{a}^n\right)_{\mathbb{R}^\mathcal{N}}=\left(\boldsymbol{Q}\boldsymbol{f}(\boldsymbol{P}^T\boldsymbol{\Psi}_r\bar{\boldsymbol{a}}^{n+1}),\boldsymbol{\Psi}_r\boldsymbol{a}^n\right)_W,$$

where $(\cdot,\cdot)_W$ denotes the Euclidean $\boldsymbol{W}$-weighted inner product in $\mathbb{R}^{\mathcal{N}}$.

The reduced order system (3.16) can be efficiently solved by the following algorithm.

Algorithm 3.2. Algorithm of SAV/BDF2-PODG-DEIM reduced system

Require: Coefficient vectors set of POD basis $\boldsymbol{\Psi}_r=[\boldsymbol{\psi}_1,\ldots,\boldsymbol{\psi}_r]$, and DEIM basis $\boldsymbol{U}=[\boldsymbol{u}_1,\ldots,\boldsymbol{u}_p]$.
Precompute $\boldsymbol{H}=\boldsymbol{\Psi}_r^T\boldsymbol{W}\boldsymbol{U}(\boldsymbol{P}^T\boldsymbol{U})^{-1}$.

1: Given the initial condition $\boldsymbol{a}^0$ and s^0 and the first step solutions $\boldsymbol{a}^1$ and s^1 computed by a first order method.
Then for $n=1,2,\ldots$, do:

2: Set $\bar{\boldsymbol{a}}^{n+1}=2\boldsymbol{a}^n-\boldsymbol{a}^{n-1}\quad \bar{\mathcal{F}}_r^{n+1}=\int_\Omega F(\Psi_r\bar{\boldsymbol{a}}^{n+1})d\boldsymbol{x}+C_0.$

3: **if** use PODG ROM **then**

4: compute coefficient $\bar{\boldsymbol{f}}_r^{\,n+1}$ by: $\boldsymbol{f}(\boldsymbol{\Psi}_r\bar{\boldsymbol{a}}^{n+1})=\boldsymbol{\Psi}_r\bar{\boldsymbol{f}}_r^{\,n+1}$.

5: **else**

6: **if** use PODG-DEIM ROM **then**

7: compute coefficient $\bar{\boldsymbol{f}}_r^{\,n+1}:=\boldsymbol{H}\boldsymbol{f}(\boldsymbol{P}^T\boldsymbol{\Psi}_r\bar{\boldsymbol{a}}^{n+1})$.

8: **end if**

9: **end if**

10: Set $\alpha_0=(\bar{\boldsymbol{f}}_r^{\,n+1},4\boldsymbol{a}^n-\boldsymbol{a}^{n-1})/3,\quad \alpha_1=\dfrac{4s^n-s^{n-1}}{3\sqrt{\bar{\mathcal{F}}_s^{n+1}}}-\dfrac{\alpha_0}{2\bar{\mathcal{F}}_s^{n+1}}.$

11: Solve $\left(\dfrac{3}{2\gamma\Delta t}\boldsymbol{I}+\boldsymbol{G}\right)\boldsymbol{u}_s^{n+1}=\bar{\boldsymbol{f}}_r^{\,n+1}.$

12: Solve $\left(\dfrac{3}{2\gamma\Delta t}\boldsymbol{I}+\boldsymbol{G}\right)\boldsymbol{w}_s^{n+1}=\dfrac{4\boldsymbol{a}^n-\boldsymbol{a}^{n-1}}{2\gamma\Delta t}-\alpha_1\bar{\boldsymbol{f}}_s^{n+1}.$

13: Compute $\alpha_2=(\bar{\boldsymbol{f}}_r^{\,n+1},\boldsymbol{u}_s^{n+1}),\quad \alpha_3=(\bar{\boldsymbol{f}}_r^{\,n+1},\boldsymbol{w}_s^{n+1}),\quad \alpha_4=\alpha_3/(2\bar{\mathcal{F}}_s^{n+1}+\alpha_2).$

14: Compute $\boldsymbol{a}^{n+1}=\boldsymbol{w}_s^{n+1}-\alpha_4\boldsymbol{u}_s^{n+1},\quad s^{n+1}=\dfrac{4s^n-s^{n-1}}{3}+\dfrac{(\bar{\boldsymbol{f}}_r^{\,n+1},\boldsymbol{a}^{n+1})-\alpha_0}{2\sqrt{\bar{\mathcal{F}}_s^{n+1}}}.$

4 Numerical results

In this section, we first present a numerical example to show the computed results of the original discretization method (i.e., the full order system) and the reduced order method in terms of stability and accuracy. We then use the proposed POD to simulate a 2D benchmark problem for the Allen-Cahn equation to demonstrate the advantage of the reduced order method. In all examples, the snapshots are calculated by the full order system (3.11).

Example 4.1. Consider the problem (1.1) in the domain $\Omega=]-1,1[^2$ with $\varepsilon=1$ and a given source term $g(x,y,t)$, so that the problem admits the exact solution $\phi=(1-x^2)^2(1-y^2)^2\sqrt{x^2+y^2+t+1}$.

We first verify the convergence rate of the time stepping scheme. To this end we use polynomial degree 32×32 for the spatial discretization, which is large enough so that the spatial discretization error is negligible compared to the temporal error. Figure 1 shows the $L^2(\Omega)$-errors of the numerical solution computed at $T=2.0$ as a function of the time step size in log-log scale. It is clearly shown that the time stepping scheme used to produce the FOS is exactly of second order as expected.

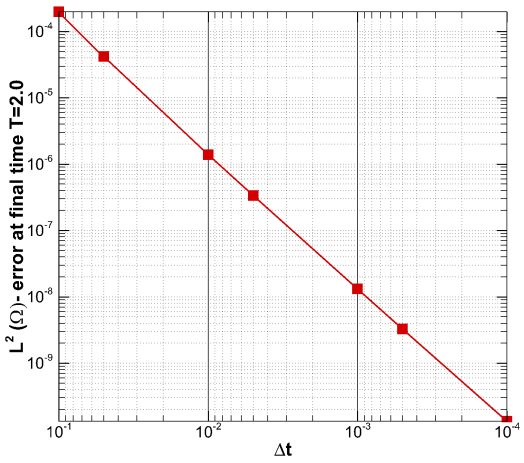

Figure 1: L^2-errors at $T=2.0$ with respect to the time step size Δt in log-log scale.

Then we investigate the POD error behavior. We collect 200 snapshots, which is a set of the numerical solutions of the FOS, i.e., (3.11) with $\Delta t=0.01$. The POD basis functions are constructed from these 200 snapshots by solving the minimization problem (2.1). In Figure 2a we present the POD error versus the POD mode number, where the POD error is defined in the left hand side of (2.4). Also shown is the singular values of the snapshot matrix, which are equal to the square root of the eigenvalues of the matrix K. By virtue of the error formula given in (2.4), the POD error is closely related to the singular values of the snapshot matrix. This is confirmed in Figure 2a, indicating that the singular values decay rapidly and the POD errors decay in a similar rate as the POD mode number, i.e., r increases. The accuracy of the POD process applied to the nonlinear term is shown in Figure 2b. In this figure we compare the POD errors with and without DEIM algorithm. It is observed that the DEIM algorithm used to reduce the computational complexity has not a significant effect on the accuracy, and both POD errors with and without DEIM have a similar decay rate as the singular values. Another remarkable point observed in Figure 2 is that the POD with 8 modes ($r=8$) gives already a very good approximation. This last observation suggests use of 8 POD modes and 8 DEIM modes in the tests that follow.

In Figure 3 we compare the L^2-error at $T=2.0$ as a function of the time step size,

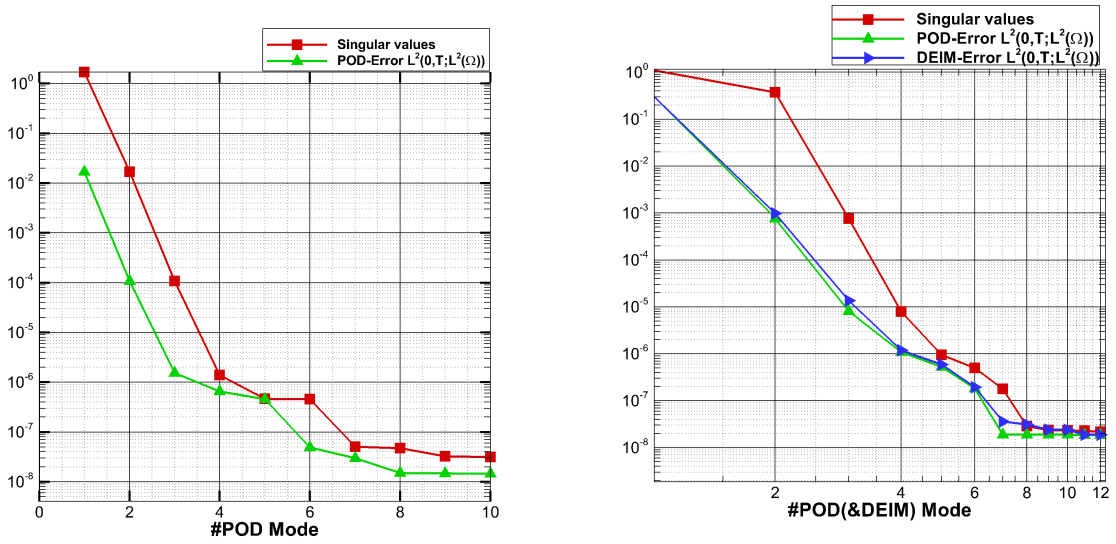

(a) (b)

Figure 2: (a) Singular values and POD L^2-errors with respect to the number of POD modes; (b) Same as (a) but for POD and DEIM algorithm applied to the nonlinear term.

obtained respectively by the ROM without and with DEIM algorithm using 8 PODG and 8 DEIM modes. The ROM is built by POD using 200 snapshots computed by FOS with $\Delta t = 0.01$. It is seen from this figure that the effect DEIM algorithm on the accuracy of the POD solution is negligible.

Example 4.2. We consider a benchmark problem for the Allen-Cahn equation (1.1) that we describe below; see also [6]. Assume at the initial state, there is a circular phase interface of the radius $R_0 = 100$ in the rectangular domain $]-128,128[^2$. Precisely, we consider the following initial condition:

$$\phi(\boldsymbol{x},0) = \begin{cases} 1, & |\boldsymbol{x}|^2 < 100^2, \\ -1, & |\boldsymbol{x}|^2 \geq 100^2. \end{cases}$$

It has been known that such a circular interface is unstable and the driving force will make it shrink and disappear. In the limit that the radius of the circle is much larger than the interfacial thickness, the interface will move at the velocity (see [1])

$$V = \frac{dR}{dt} = -\frac{1}{R}.$$

The radius of the moving interface evolves as $R(t) = \sqrt{R_0^2 - 2t}$. In the implementation we map the computational domain $]-128,128[^2$ to $]-1,1[^2$. Doing so we are led to solve the

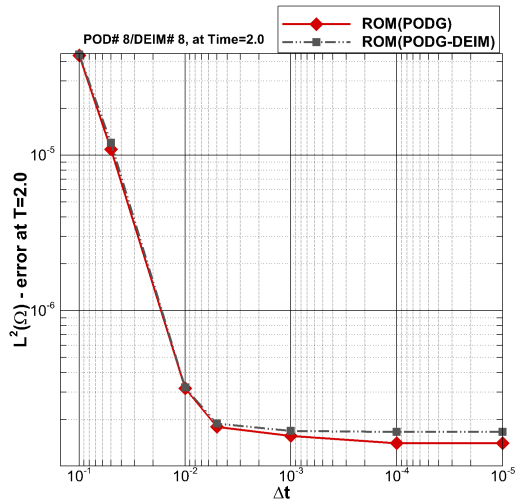

Figure 3: The comparison of the errors at $T=2.0$ between FOS and the POD with 8 POD modes and 8 DEIM modes using the snapshots with $\Delta t=0.01$.

Allen-Cahn equation (1.1) with the coefficients $\gamma=1/128^2$ and $\varepsilon=0.0078$, where ε appears in front of the nonlinear term. The FOS becomes stiff for the small ε because the interface becomes thin for small parameters and fine resolution is needed around the interface. In the simulation, the space grid is taken as 512×512, and the time-step size is $\Delta t=0.1$. The computed radius $R(t)$ using the SAV/BDF2 scheme is plotted in Figure 4. We observe

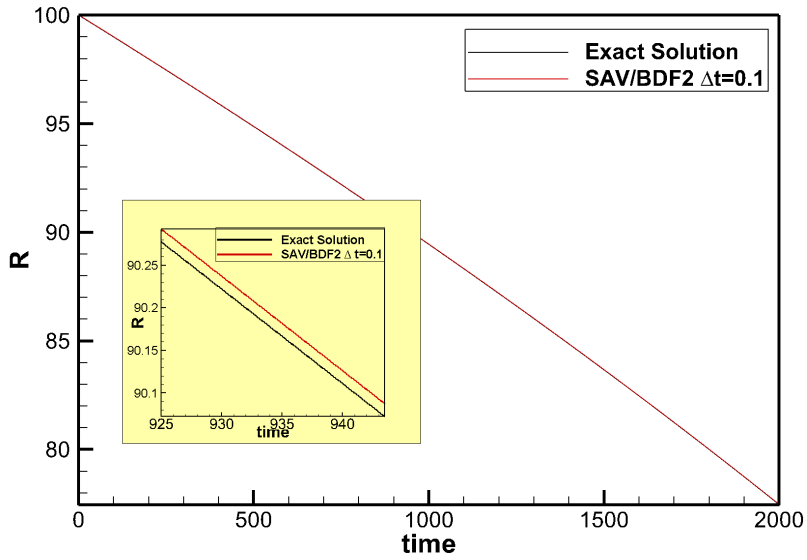

Figure 4: The evolution of radius $R(t)$ for Benchmark problem: comparison of the exact solution and numerical result computed by FOS with $N_x=N_y=512$.

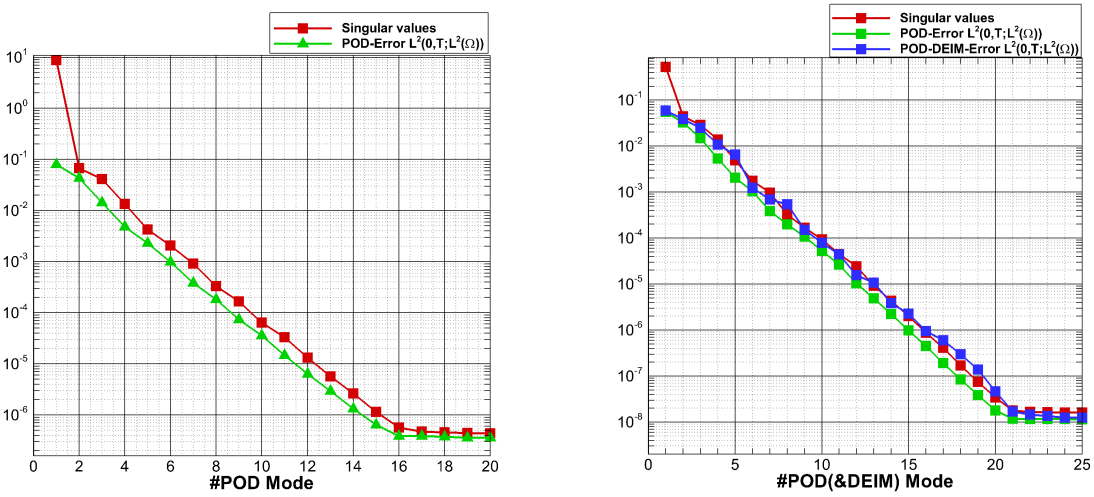

(a) (b)

Figure 5: Benchmark problem: (a) singular values and POD L^2-errors with respect to the number of POD modes; (b) Same as (a) but for POD and DEIM algorithm applied to the nonlinear term.

that $R(t)$ keeps monotonously decreasing at a rate very close to the sharp interface limit value. This demonstrates the accuracy of the FOS.

The singular values and POD errors are also computed for this example, and the results are shown in Figure 5. Here the POD basis and DEIM basis are constructed by 200 snapshots, which are solutions of FOS with $\Delta t=0.1$ at 200 different instants. The singular values and relative $L^2(0,T;L^2(\Omega))$ errors versus different numbers of POD modes are given in Figure 5a. It is observed that the singular values and POD errors decay at a similar rate as POD mode number increases. Figure 5b shows the result of POD-DEIM method for the nonlinear term, leading to a similar observation.

An accuracy comparison of the POD without DEIM and POD with DEIM is shown in Figure 6, where the L^2-errors at $T=20.0$ as functions of the time step size are plotted. The POD (and DEIM) make use of 16 POD modes and 21 DEIM modes, and the errors are measured by using the "reference solution" provided by the FOS. We see that both POD and POD-DEIM produce accurate enough solutions.

Finally, in Table 1, we present the average CPU times at each time step for the FOS, POD method with 16 modes without DEIM, and POD-DEIM with 21 modes. The speed-up factors compared to FOS are also listed for POD and POD-DEIM. It is clearly observed that the POD method efficiently speed up the calculation, and the DEIM for the nonlinear term further improves the computational efficiency.

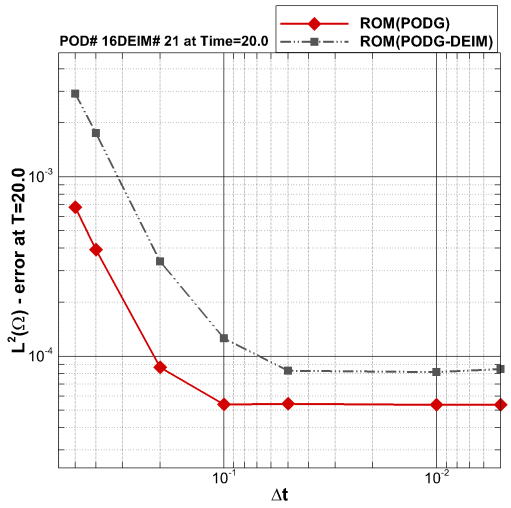

Figure 6: Comparison of $L^2(\Omega)$-errors at $T=20.0$ between the ROM without DEIM and ROM with DEIM using 16 POD modes and 21 DEIM modes.

Table 1: Average CPU time for each time step.

	FOS	ROM with 16POD	ROM with 16POD-21DEIM
t_{cpu}(sec)	2.36	0.45	0.12
Speed-up Factor		5.24	19.67

5 Conclusions and perspectives

We have developed a reduced-order model for the Allen-Cahn equation. At first, we constructed a numerical method based on SAV approach for the time stepping scheme and a spectral-Galerkin method for the space discretization. Then the constructed numerical method was used to product preliminary phase field data, i.e., an ensemble of snapshots of at some time instants. Based on these phase field data, the reduced order model is derived by Proper Orthogonal Decomposition (POD) for the construction of the reduced basis, and Discrete Empirical Interpolation Method (DEIM) for dealing with the nonlinear term. Finally, a same SAV based second-order unconditionally stable time stepping scheme is applied to yield the reduced order system. Several numerical examples were provided to demonstrate the efficiency of the proposed POD and POD-DEIM. In particular, the obtained numerical results showed that the reduced order model gave good approximations to the full order system and achieve substantial improvement in efficiency as compared to directly solving the full order system. It is worthy to emphasize that the proposed method can be extended to solve other kinds of gradient flow problems.

Acknowledgments

The work was supported by NSFC/ANR joint program 51661135011 - PHASEFIELD. The second author has received financial support from the French State in the frame of the "Investments for the future" Programme Idex Bordeaux, reference ANR-10-IDEX-03-02. The third author was supported by NSFC projects 11971408, 51661135011, 11421110001, and 91630204.

References

[1] S.M. Allen and J.W. Cahn. A microscopic theory for antiphase boundary motion and its application to antiphase domain coarsening. *Acta Metallurgica*, 27:1085–1095, 1979.

[2] J. Baiges, R. Codina and S. Idelsohn. Explicit reduced-order models for the stabilized finite element approximation of the incompressible Navier-Stokes equations. *J. Numer. Methods Fluids*, 72:1219–1243, 2013.

[3] G. Berkoz, P. Holmes and J.L. Lumley. The proper orthogonal decomposition in the analysis of turbulent flows. *Annu. Rev. Fluids Mech.*, 25:539–575, 1993.

[4] J. Burkardt, M. Gunzburger and H.-C. Lee. POD and CVT-based reduced-order modeling of Navier-Stokes flows. *Comput. Methods Appl. Mech. Engrg.*, 196:337–355, 2006.

[5] S. Chaturantabut and D. Sorensen. Nonlinear model reduction via discrete empirical interpolation. *SIAM Journal on Scientific Computing*, 32:2737–2764, 2010.

[6] L.Q. Chen and J. Shen. Applications of semi-implicit fourier-spectral method to phase field equations. *Computer Physics Communications*, 108(2):147–158, 1998.

[7] M.O. Deville, P.F. Fischer and E.H. Mund. *High-Order Methods for Incompressible Fluid Flow, Cambridge University Press*. Cambridge University Press, Cambridge.

[8] I. Kalashnikova and M. F. Barone. Efficient non-linear proper orthogonal decomposition/Galerkin reduced order models with stable penalty enforcement of boundary conditions. *Internat. J. Numer. Methods Engrg.*, 90:1337–1362, 2012.

[9] K. Kunisch and S. Volkwein. Galerkin proper orthogonal decomposition methods for parabolic problems. *Numer. Math.*, 90:117–148, 2001.

[10] J. Shen, T. Tang and L. Wang. *Spectral Methods: Algorithms, Analysis and Applications, Springer Series in Computational Mathematics*. 2011.

[11] J. Shen and J. Xu. Convergence and error analysis for the scalar auxiliary variable (SAV) schemes to gradient flows. *SIAM Journal on Numerical Analysis*, 56:2895–2912, 2018.

[12] M. Uzunca and B. Karasözen. Energy Stable Model Order Reduction for the Allen-Cahn Equation. In: *P. Benner, M. Ohlberger, A. Patera, G. Rozza and K. Urban (eds.) Model Reduction of Parametrized Systems.* Springer International Publishing, Cham, pp.403–419, 2017.

[13] S. Volkwein. Proper orthogonal decomposition: theory and reduced-Order modelling. Lecture Notes, University of Konstanz, Available at: *http://www.math.uni-konstanz.de/numerik/personen/volkwein/teaching/POD-Book.pdf*. 2013.

[14] J. Shen and J. Xu. The scalar auxiliary variable (SAV) approach for gradient flows. *Journal of Computational Physics*, 353:407–416, 2018.

[15] Huailing Song, Lijian Jiang and Qiuqi Li. A reduced order method for Allen-Cahn equations. *Journal of Computational and Applied Mathematics*, 292:213–229, 2016.

[16] D. Chapelle, A. Gariah and J. Sainte-Marie. Galerkin approximation with proper orthogonal decomposition: new error estimates and illustrative examples. *ESAIM Math. Model. Numer. Anal.*, 46:731–757, 2012.